Electronic supplementary information

Magnetic Fe$_3$O$_4$@polyaniline nanocomposites with tunable core-shell structure for ultrafast microwave-energy-driven reduction of Cr(VI)
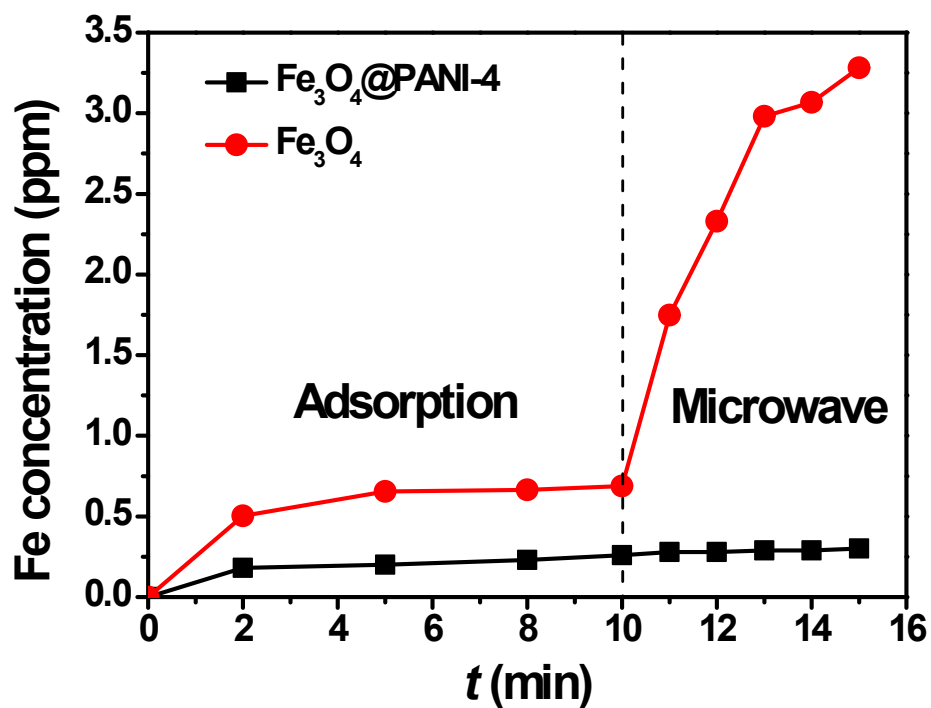
Changqing Zhu[1], Fuqiang Liu*[1], Li Song[1], Hao Jiang[1] and Aimin Li[1]

[1]State Key Laboratory of Pollution Control and Resources Reuse, School of the

Environment, Nanjing University, Nanjing 210046, P.R.China

* Corresponding author: Tel: +86 139 1387 1032; Fax: +86 25 89680377; Email

address: jogia@163.com

Figure S1. Acid resistance of Fe$_3$O$_4$@PANI

Figure S1. Concentration change of Fe in bulk solution from Fe$_3$O$_4$@PANI-4 and Fe$_3$O$_4$. Dosage: Fe$_3$O$_4$@PANI-4, 10 mg; Fe$_3$O$_4$, 4.485 mg to match the Fe content in Fe$_3$O$_4$@PANI-4, pH=2, solution volume=50 mL.

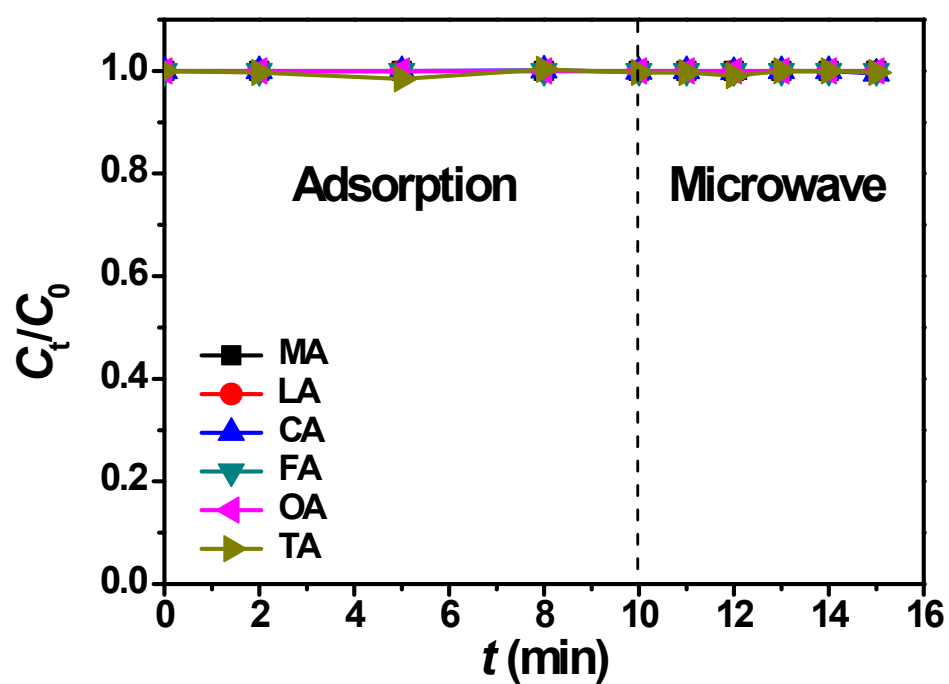**Figure S2.** Cr(VI) removal without Fe₃O₄@PANI-4

Figure S2. Cr(VI) removal in Adsorption stage and MW stage with various organic acids as sacrificial electron donors in the absence of Fe$_3$O$_4$@PANI-4.

Table S1 Structures and physicochemical parameters of various low-molecule-weight organic acids.
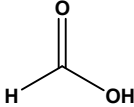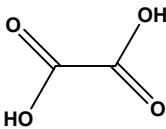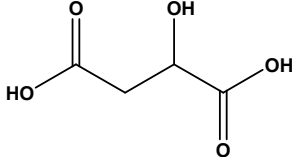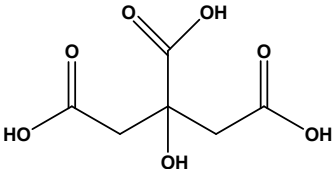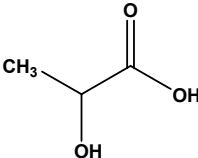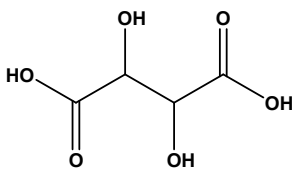
Acid	Structure	pK_a	E_{HOMO}	$k_{obs,a}$	k_a
Formic acid		3.77	-0.2562	0.31157	0.04929
Oxalic acid		1.23	-0.252	0.57733	0.31505
Malic acid		3.40	-0.2458	0.33187	0.06959
Citric acid		3.09	-0.2441	0.36698	0.1047
Lactic acid		3.86	-0.2409	0.38927	0.12699
Tartaric acid		2.89	-0.2368	0.4713	0.20902

Figure S3. Change of solution pH during Adsorption stage and MW stage

Figure S3. Change of solution pH during Adsorption stage and MW stage.

Figure S4. Cr species distribution

Figure S4. Species distribution of (a) Cr(VI) and (b) Cr(III) depending on solution pH.

Figure S5. Effect of aqueous chemistry parameters and MW power

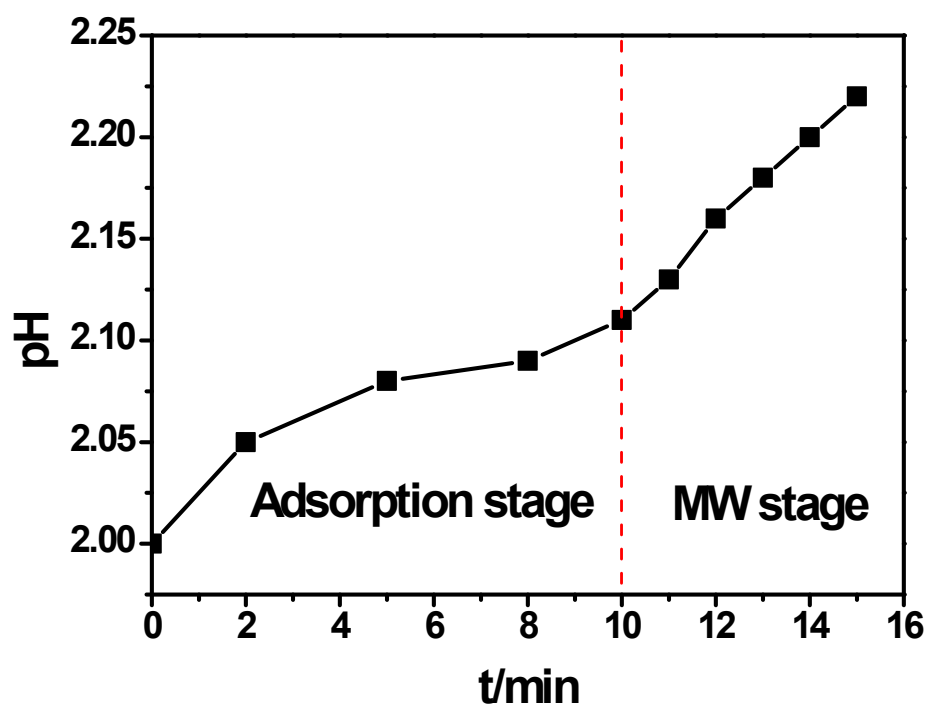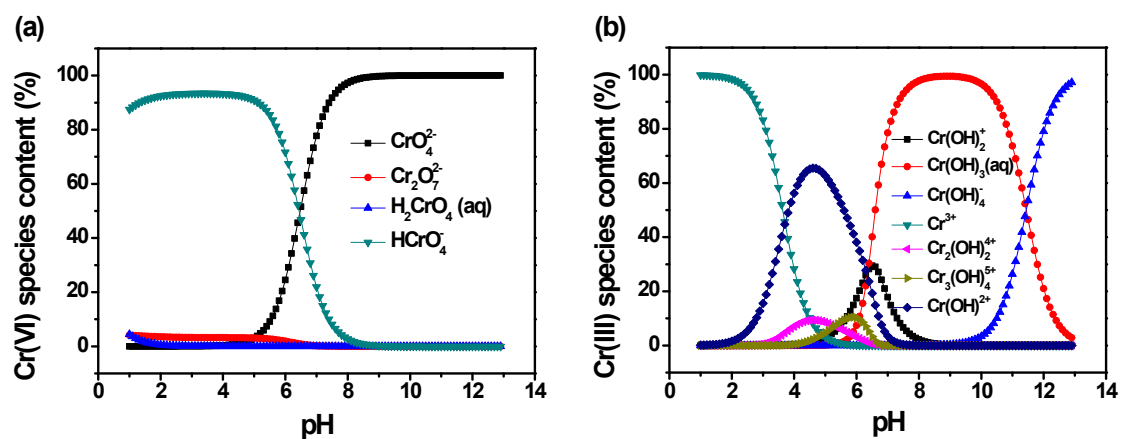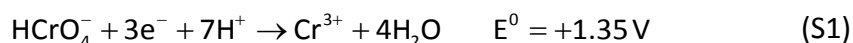The adsorption and reduction of Cr(VI) were influenced by a series of reaction parameters. Herein, the effects of pH, Cr(VI) and acid concentrations and MW power were investigated with OA as the sacrificial electron donor. Figure S5a showed that the removal ratio of Cr(VI) in Adsorption stage (R_{ads}) decreased monotonously from 42.43% to 7.43% in the pH range of 2-10 at the initial Cr(VI) concentration of 1.0 mmol/L. According to the species simulation (Figure S4), $HCrO_4^-$ predominated at pH between 2 and 6.5 while CrO_4^{2-} dominated at pH above 6.5. Thus, the decline of R_{ads} was attributed to the increase of CrO_4^{2-} species, which required two ion-exchange sites for binding whereas $HCrO_4^-$ required one, as well as to the site competition from the increasing OH^- when pH increased. Besides, the deprotonation process of amino groups also decreased the amount of positive-charged sites for electrostatic interaction.[1]

After MW was introduced, the surface-bound Cr(VI) was rapidly reduced which consumed lots of protons as Eq.(S1) and (S2):[2]

$$HCrO_4^- + 3e^- + 7H^+ \rightarrow Cr^{3+} + 4H_2O \qquad E^0 = +1.35\,V \qquad (S1)$$

$$CrO_4^{2-} + 3e^- + 8H^+ \rightarrow Cr^{3+} + 4H_2O \qquad E^0 = +1.48\,V \qquad (S2)$$

The increased pH decreased the amounts of surface-bound Cr(VI) and protons available for the reduction reaction. Meanwhile, pH rise also declined the thermodynamic driving force for reduction of Cr(VI), which was related with the potential difference between the Cr(VI)/Cr(III) redox couple ($E^o(Cr^{6+}/Cr^{3+})$).[3] Herein, the total Cr(VI) removal in Adsorption & MW stages was donated as R_{ads+MW} and the net removal ratio of Cr(VI) in MW stage was donated as R_{MW}, which could be calculated as $R_{MW}=R_{ads+MW}-R_{ads}$. Increasing pH depressed the reduction of Cr(VI) in MW stage, resulting in less adsorption sites being released and thereby the lowered R_{MW} values. It was noted that R_{MW} changed from positive values of 49.21%, 34.06%, 7.43% for pH of 2.0, 2.3, 3.0 to negative values of -3.72%, -3.41%, -2.48%, -2.79% for pH of 4.0, 5.0, 7.0, 10.0, implying that surface-bound Cr(VI) were desorbed by MW in high pH range. According to the stoichiometry in Eq.(S1) and (S2), over one proton were consumed to reduce one Cr(VI). Afterwards, an alkaline microdomain was generated within the interface, followed by being neutralized by protons from (i) acidic bulk solution or (ii) deprotonation of H^+-bearing adsorption sites (e.g. $-NH_2^+-$). At low pH, the protons in bulk solution were adequate to supplement the consumed protons while at high pH, the deprotonation process became dominated, leading to the release of Cr(VI) from surface sites. As a result, the net effect of MW on Cr(VI) removal, reflected by R_{MW} values, changed from positive to negative. Consequently, R_{ads+MW} decreased from 91.64% to 4.64% as increasing pH from 2 to 10.

When the initial Cr(VI) concentration decreased to 0.2 mmol/L, the same trends of R_{ads}, R_{MW} and R_{ads+MW} were observed (Figure S5b). However, the pH where R_{MW} changed from positive to negative right shifted from 4.0 to 5.0. The pH below which over 90% of R_{ads+MW} was obtained also right shifted from 2.0 to 3.0 because less

protons were required to reduce low concentration of Cr(VI), suggesting that the Fe$_3$O$_4$@PANI/MW process was also effective for treating contaminated water with low Cr(VI) concentration and acidity.

Figure S5c displayed the influence of OA concentration on Cr(VI) removal in Adsorption and MW stages. Increasing OA contents from 0 to 2.0 mmol/L improved R_{ads}, R_{MW} and R_{ads+MW} values with a increment of 12.62%, 14.19% and 26.81%, respectively, resulting from the enhanced Cr(VI) reduction at higher sacrificial reductant concentrations. In Figure S5d, over 97% of R_{ads+MW} was accomplished even when MW power declined from 900 W to 540 W. Then R_{ads+MW} decreased to 81.93% and 41.43% when MW power further dropped to 360 W and 180 W, respectively.
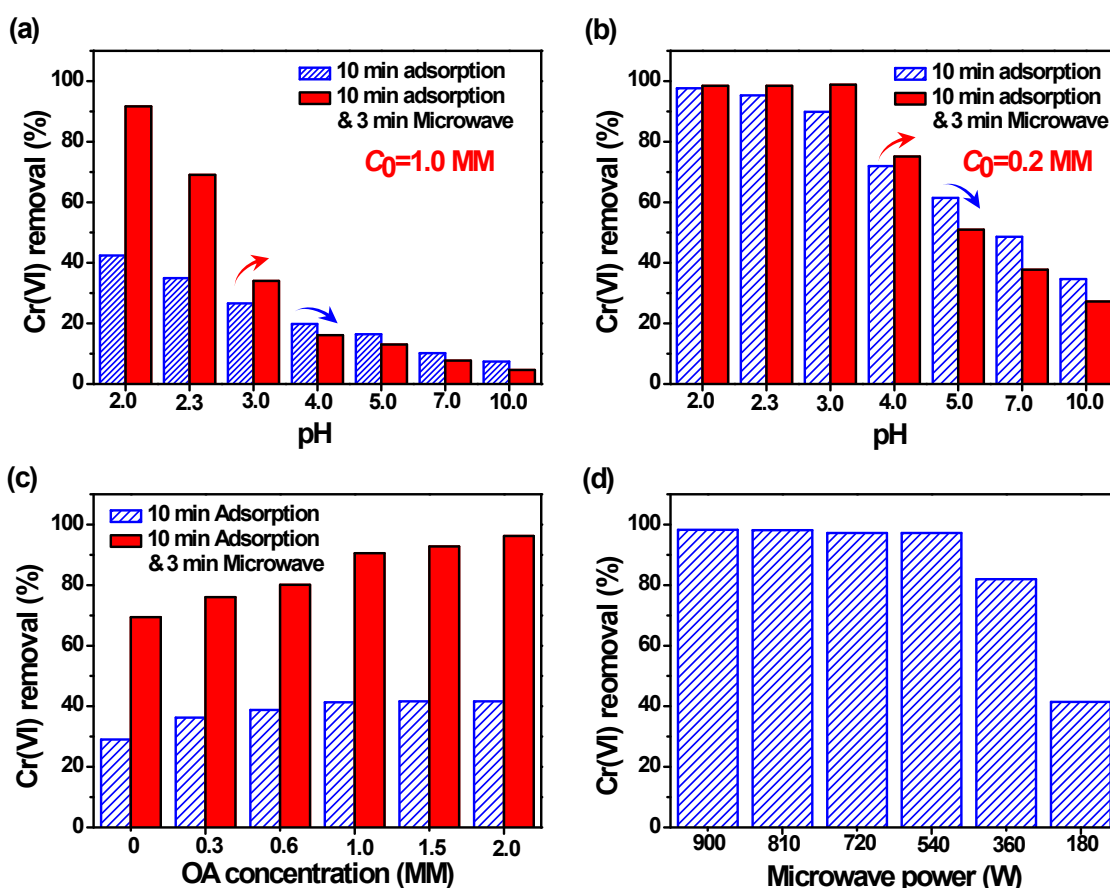

Figure S5. Effect of pH on Cr(VI) removal at initial Cr(VI) concentrations of (a) 1.0 mmol/L and (b) 0.2 mmol/L; (c) Effect of OA concentrations on Cr(VI) removal (Cr(VI), 1.0 mmol/L); (d) Effect of MW power on Cr(VI) removal (Cr(VI), 1.0 mmol/L).

Figure S6. Temperature profile of the bulk solution under 900 W microwave irradiation

The temperature profile of the bulk solution under 900 W microwave irradiation has been recorded as Figure S6. After microwave irradiation started, the solution temperature increased quickly and reached 100 °C at 100 s, then kept constant in the following time.
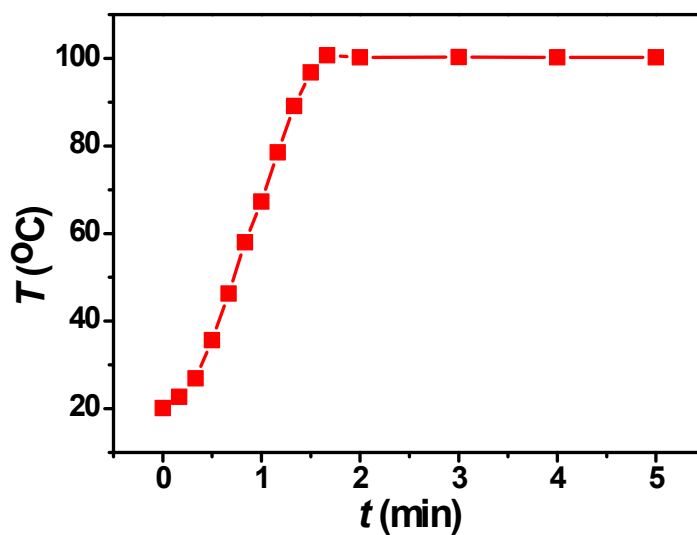
Figure S6. Temperature profile of the bulk solution under 900 W microwave irradiation.

Figure S7. Concentration change of Cr(VI) in Adsorption stage, and MW-assisted and non MW-assisted (external heating) processes

The maximum temperature reached in the MW process was 100 °C, which was then used as the temperature where non MW-assisted test was conducted. After adsorption for 10 mins, the catalyst was separated from the bulk solution by a magnet. Then the bulk solution was transferred into a hot oil bath (105 °C) and heated to boil (100 °C). Afterwards, the hot solution was immediately poured into the catalyst-containing bottle, which was continually heated in the above oil bath. The concentration change of Cr(VI) was recorded as Figure S7. Compared to that in the MW-assisted process, Cr(VI) concentration decreased with a much slower rate in the external heating process at 100 °C, suggesting that higher efficiency of MW irradiation by generating hot spots for Cr(VI) reduction.
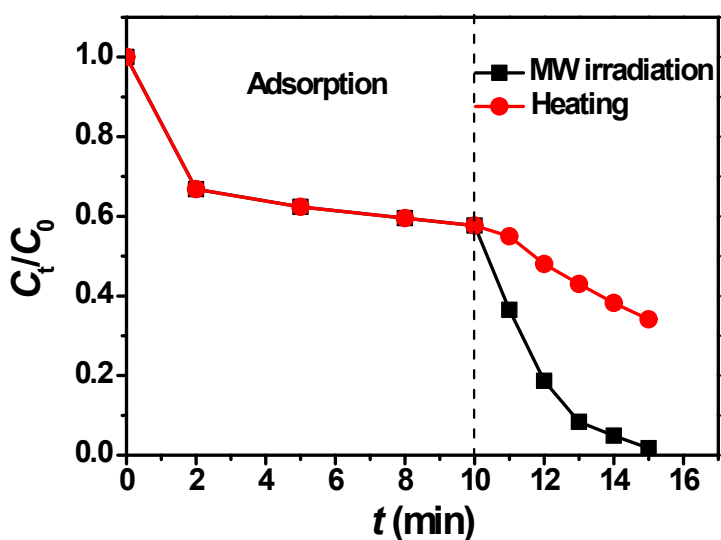
Figure S7. Concentration change of Cr(VI) in Adsorption stage, and MW-assisted and non MW-assisted (external heating) processes.

Figure S8. Removal of Cr(VI) by non magnetic PANI and magnetic Fe_3O_4@PANI-4 in Adsorption and Microwave stages.

The non magnetic PANI was prepared by using strong hydrochloric acid (weight ratio, 6.75%) to dissolve the Fe_3O_4 core for 2 h at 95 °C. Then the resulted PANI shell was rinsed in dilute sulfuric acid solution (pH=1) for 6 h to exchange the adsorbed Cl^-. Afterwards, the PANI shell was washed by ultrapure water until neutral pH and dried for further use. The result of Cr(VI) removal using the non magnetic PANI was shown in Figure S8. The Cr(VI) removal performances of Fe_3O_4@PANI-4 in both Adsorption and Microwave stages were declined after the Fe_3O_4 core was dissolved. The strong acid treatment possibly caused the collapse of the hollow PANI shell, which screened part of adsorption sites and decreased the adsorption capacity. Meanwhile, as the Fe_3O_4 core could effectively harvest microwave energy, the removal of it resulted in the weakened microwave absorbing, thus producing less hot spots to accelerate Cr(VI) reduction. Therefore, the removal rate of Cr(VI) by non magnetic PANI within microwave field was slower than that by Fe_3O_4@PANI-4. That is, there is a synergy between Fe_3O_4 and PANI in the microwave process.
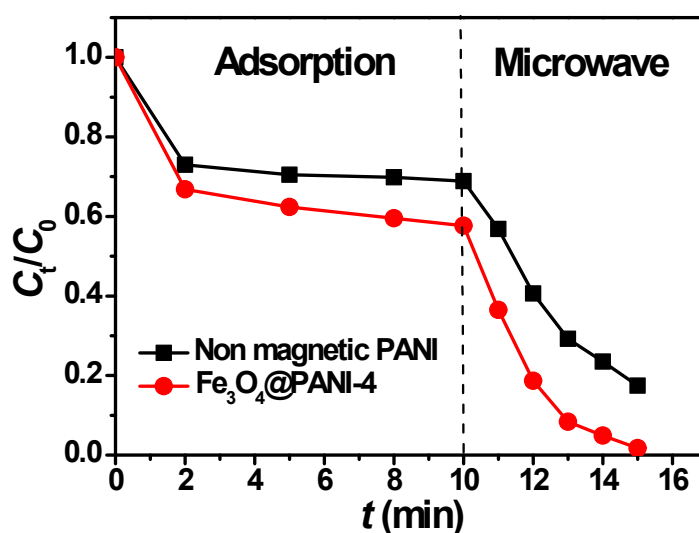
Figure S8. Removal of Cr(VI) by non magnetic PANI and magnetic Fe_3O_4@PANI-4 in Adsorption and Microwave stages.

References

1 B. Qiu, C. Xu, D. Sun, H. Yi, J. Guo, X. Zhang, H. Qu, M. Guerrero, X. Wang, N. Noel, Z. Luo, Z. Guo and S. Wei, *ACS Sustain. Chem. Eng.*, 2014, **2**, 2070-2080.

2 N. Wang, L. Zhu, K. Deng, Y. She, Y. Yu and H. Tang, *Appl. Catal. B: Environ.*, 2010, **95**, 400-407.

3 C. Zhu, F. Liu, Y. Zhang, M. Wei, X. Zhang, C. Ling and A. Li, *Chem. Eng. J.*, 2016, **306**, 579-587.